Predictive Control of Five-leg Inverter Driving Dual PMSMs for Overcurrent Suppression

Chen, Yong; Dong, Zhiping; Song, Zaixin; Liu, Chunhua

Published in:
IEEE Transactions on Industry Applications

Published: 01/09/2024

Document Version:
Post-print, also known as Accepted Author Manuscript, Peer-reviewed or Author Final version

Published version (DOI):
10.1109/TIA.2024.3420821

Publication details:
Chen, Y., Dong, Z., Song, Z., & Liu, C. (2024). Predictive Control of Five-leg Inverter Driving Dual PMSMs for Overcurrent Suppression. *IEEE Transactions on Industry Applications*, *60*(5), 6949-6958. https://doi.org/10.1109/TIA.2024.3420821

Chen, Y., Dong, Z., Song, Z., & Liu, C. (2024). Predictive Control of Five-leg Inverter Driving Dual PMSMs for Overcurrent Suppression. *IEEE Transactions on Industry Applications, 60*(5), 6949-6958. https://doi.org/10.1109/TIA.2024.3420821

Predictive Control of Five-leg Inverter Driving Dual PMSMs for Overcurrent Suppression

Yong Chen, Zhiping Dong, Zaixin Song, and Chunhua Liu*, *Senior Member*, *IEEE*

***Abstract*—The five-leg inverter has been investigated widely as a low-cost solution for dual permanent magnet synchronous motors (PMSMs) drives. It installs a common leg between dual PMSMs and can be considered a fault-tolerant approach in the event of an open-circuit fault occurring within an inverter leg. For this topology, the overcurrent of the shared leg should be handled carefully since the confluence of phase current naturally amplifies the current peak. In this article, an enhanced model predictive control (MPC) scheme is presented to realize cooperative dual-PMSMs control, effective overcurrent elimination, lower computational burden, and fast transient response simultaneously. The master-slave structure and deadbeat control-based duty cycle partitioning scheme are adopted to eliminate the switching state conflict on the common leg and realize independent current controller construction. In addition, the relations of current phases of dual PMSMs are deduced, designed, and utilized to modify the reference current of the slave motor. As a result, the overcurrent component is contained in the cost function directly. Finally, the experimental tests of a dual-PMSM system are executed, and the results substantiate the effectiveness and superiority of the proposed algorithm.**

***Index Terms*—Cost function, dual motors, five-leg inverter, model predictive control, overcurrent suppression.**

I. INTRODUCTION

DUAL-MOTOR systems exhibit elevated power output, strong robustness, and enhanced control flexibility. Consequently, they have been extensively employed across a myriad of industrial applications [1], [2], [3]. In [4], an optimal coordinated control method is introduced to drive a dual-motor gear transmission system. An overmodulation strategy for torque balance considering angle offset is introduced for dual permanent magnet synchronous motors (PMSMs) systems in [5]. Moreover, in [6], a two-rotor axial-flux machine is designed to realize equivalent function of dual motors for underwater propulsion. In these applications, the dual-PMSMs five-leg voltage source inverter (FL-VSI) drive is a classical topology for system cost reduction [7], [8]. Also, it is considered a fault-tolerant approach in the case of an open-circuit fault in an inverter leg [9]. Compared to other topologies, such as four-leg VSI [10] and three-leg dual parallel drive topology [11], it retains a larger degree of freedom of control and is especially applicable to non-rigidly connected dual-motor systems.

In decades, numerous control strategies have been put forward to drive dual motors independently on FL-VSI, such as hysteresis current control [12], field-oriented control with PI controller [13], model predictive control (MPC) [14], and sensorless control [15]. In [12], a simple dual-level hysteresis current control strategy is developed to control a dual-PMSM system without any motor parameters. In [13], an improved pulse width modulation method is proposed to expand the speed ranges of two motors. In [16], a current reconstruction method is introduced to further reduce volume and enhance the robustness of system via a single current sensor. Moreover, the method for FL-VSI drives can be further extended to multiple-motor control for higher power requirements [17].

Among all methods, the MPC-based strategies possess the merits of simple structure, flexible cost function, and fast dynamic response [18], [19], [20]. Therefore, they have received more and more attention. For example, Lim *et al*. proposed several MPC-based methods and conducted a comparative study [14], [21]. The traditional method considering dual-motor control into an integrated cost function yields a large computational burden. To this end, the traverse process of candidate vectors should be optimized. A classical improvement is to separate the control cycle into two intervals according to voltage demands, and one per motor [22]. In each interval, the related current controller only tests seven basic voltage vectors (VVs), but the method decreases voltage utilization inevitably. In addition, another priority-based method is introduced in [23] for driving dual induction motors. It traverses the total twelve VVs to decide the switching states of FL-VSI. However, the fixed amplitude of applied VV yields larger current ripple.

Moreover, the overcurrent protection should be considered carefully in MPC algorithm design. In [24], a receding horizon optimization is conducted considering overcurrent protection in model predictive speed regulation. In [25], the current and torque limits are employed as softened state constraints to calculate flux linkage reference. Wang *et al*. realize the current

Manuscript received Feb 21, 2024; revised May 12, 2024; accepted Jun 17, 2024. Paper 2024-IDC-0305.R1, presented at the 2023 IEEE 6th Student Conference on Electric Machines and Systems, Huzhou, China, Dec. 7-9. This work was supported in part by Research Fellow Scheme (Project No.: RFS2223-1S05) from Research Grants Council, Hong Kong SAR; in part by a Collaborative Research Fund (Project No. C1052-21GF) from the Research Grants Council, Hong Kong SAR; and General Research Fund (Project No.: 11217623) from Research Grants Council, Hong Kong SAR. (*Corresponding author: Chunhua Liu)

Yong Chen, Zhiping Dong, and Chunhua Liu are with the School of Energy and Environment, City University of Hong Kong, Hong Kong SAR, China. (e-mail: yong.chen@my.cityu.edu.hk; Zhiping.Dong@my.cityu.edu.hk; chunliu@cityu.edu.hk).

Zaixin Song is with the State Key Laboratory of Ultra-precision Machining Technology, Department of Industrial and Systems Engineering, Hong Kong Polytechnic University, Hong Kong SAR, China. (e-mail: zaixin.song@polyu.edu.hk).

limitation with a second-order nonlinear disturbance observer [26]. Furthermore, the limitation of peak value of phase current is included in cost function in [22], while the issue of overcurrent suppression in the common leg of FL-VSI topology has not been considered. Actually, different from the traditional overcurrent protection mechanism, the current flows into common leg may be twice as large as other legs when dual motors work in parallel. In addition, though the angle controller enables phase angle regulation to minimize the current [27], it needs extra tuning of controller parameters, and the current response is slow due to the cascaded control structure.

In this article, as an extended version of [28], an improved MPC scheme is proposed to drive dual PMSMs with the minimum current in FL-VSI. The main contributions of this work are summarized as follows.

1) By combining master-slave structure, MPC control, and duty cycle partitioning, the cooperative drive of dual motors is achieved within an affordable computational burden.

2) The current phase angle of slave motor is regulated according to that of master motor and is integrated into related cost function design to minimize overcurrent.

3) Numerous experimental results are supplemented to compare the performance of steady-state, dynamic, and algorithm complexity among the proposed method and the classical MPC schemes.

The remaining part of this article is organized as follows. Section II establishes the system model of the FL-VSI driving dual-PMSM system. Section III presents the improved MPC scheme, consisting of current phase analysis, cost function design, and control system construction. Furthermore, the experimental results are delineated in Section IV. Finally, the study is summarized in Section V.

II. System Modeling

A. PMSM Driving Model

The structure of the FL-VSI driving dual-PMSM system is shown in Fig. 1. Compared to full-switches topology, the L_5 is set as common leg that connects phase c of dual PMSMs, while phases a and b can be controlled freely. This coupled-leg topology yields extra problems when the switching states commands from the selected VVs to the shared leg are incompatible. Furthermore, because the confluence of phase current amplifies the current peak, it raises more strict demands to switch specification and protective circuit. Therefore, the control strategy of FL-VSI and overcurrent protection should be considered and adjusted optimally.

In addition, the voltage models in the d/q-axis synchronous frame are [27]

$$\begin{bmatrix} u_d \\ u_q \end{bmatrix} = \begin{bmatrix} R_s & -\omega_e L_q \\ \omega_e L_d & R_s \end{bmatrix} \begin{bmatrix} i_d \\ i_q \end{bmatrix} + \begin{bmatrix} L_d & 0 \\ 0 & L_q \end{bmatrix} \frac{\mathrm{d}}{\mathrm{d}t} \begin{bmatrix} i_d \\ i_q \end{bmatrix} + \begin{bmatrix} 0 \\ \omega_e \psi_f \end{bmatrix} \quad (1)$$

where L_d, L_q, u_d, u_q, i_d, and i_q are inductances, stator voltages, and stator currents of d/q-axis, respectively; ω_e is the electric angular velocity, R_s represents the stator resistance, ψ_f is the permanent magnet flux linkage.

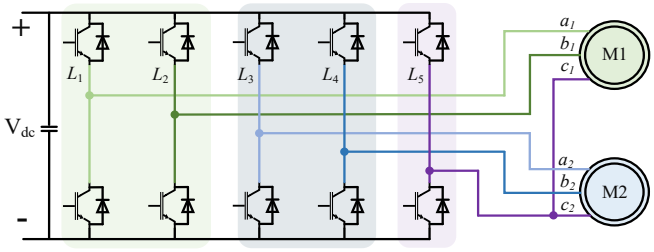

Fig. 1. Structure of FL-VSI driving dual PMSMs.

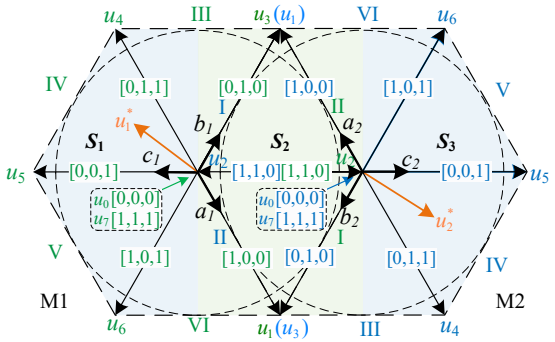

Fig. 2. Vector plane and sector division of dual PMSMs supplied from FL-VSI.

Based on (1) and applying the discretization method, the current prediction expressions are derived as follows [29]:

$$\begin{aligned} i_d(k+1) &= (1 - R_s T_s / L_d) i_d(k) + (T_s / L_d) u_d(k) \\ &\quad + (L_q \omega_e(k) T_s / L_d) i_q(k) \end{aligned} \quad (2)$$

$$\begin{aligned} i_q(k+1) &= (1 - R_s T_s / L_q) i_q(k) + (T_s / L_q) u_q(k) \\ &\quad + (-L_d \omega_e(k) T_s / L_q) i_d(k) - T_s \omega_e(k) \psi_f / L_q \end{aligned} \quad (3)$$

where (k) and $(k+1)$ are the current and the next instants, and Ts is the sampling interval of current. Based on the classical predictive theory, the candidate voltages can be traversed to select the best one to minimize the specific cost function, such as current tracking error minimization.

The torque equation and mechanical equation of PMSM can be written as

$$T_e = \frac{3}{2} p i_q [i_d (L_d - L_q) + \psi_f] \quad (4)$$

$$J * \frac{d\omega}{dt} = T_e - T_L - B\omega \quad (5)$$

where ω is the mechanical angular velocity, p is the number of pole pairs, T_e and T_L are electromagnetic torque and load torque, B is viscous friction coefficient, and J is rotor inertia.

B. VVs Selection and MPC Principle

The voltage vector plane and sector division of dual PMSMs supplied from FL-VSI are depicted in Fig. 2. The voltage hexagons of dual motors are rotated to facilitate the graphic presentation of vector limitation. Each motor has 2^3 switching states with three half-bridge inverters. The whole plane can be divided into two parts, namely blue and green areas, where the switching state of L_5 is opposite. Supposing only one basic VV is output to each motor, the selected ones should be located in the same area due to the coupling utilization of common leg of the VSI.

In addition, the control blocks of traditional MPC schemes for driving dual PMSM supplied from FL-VSI are illustrated

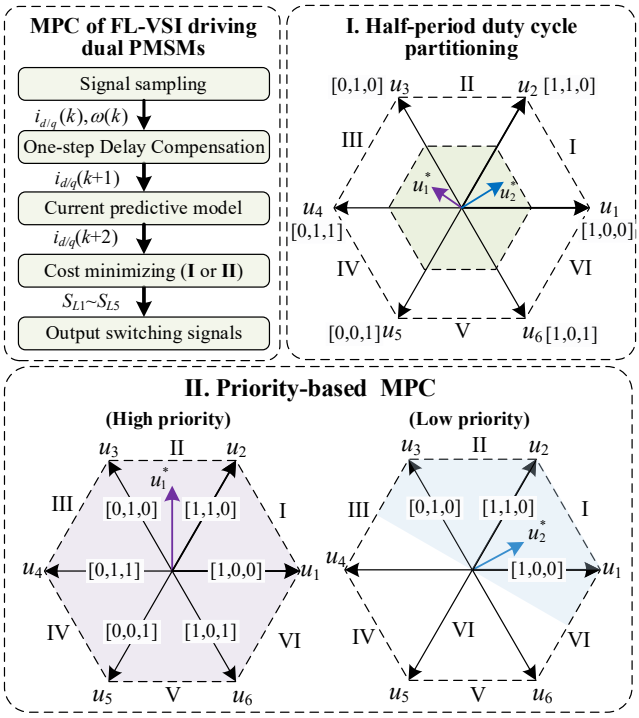

Fig. 3. Control blocks of traditional MPC schemes.

in Fig. 3. The traditional MPC scheme comprises three parts, namely delay compensation, predictive model formulation, and cost function design [27]. Compared to that of a single motor drive, the main difference of the FL-VSI driving system is the cost minimization procedure. To overcome the hardware limit from common leg, two classical improvements have been studied. In the first method, the half-period duty cycle partitioning scheme is utilized [15], and each motor is given active VVs in a partition. This scheme decouples dual-PMSM control completely at the cost of voltage utilization reduction. On the contrary, the second method is a priority-based solution that can output the full capacity of power supply [23]. It forces dual PMSMs to obtain VVs with the identical switching states of common leg, which brings about a higher current ripple. Moreover, under both improvements, the optimal VVs of dual PMSMs are selected separately with two cost functions, but the overcurrent suppression of common leg has not been contained in the cost function design.

III. Proposed Predictive Control of Dual PMSMs

In this section, the proposed predictive control scheme is introduced in a sequence encompassing current phase analysis, cost function design, and control system construction. Specifically, the dual PMSMs with the same parameters and work parallel under identical speeds are studied in the paper.

A. Current Phase Analysis

The phase current of PMSM can be written as

$$\begin{cases} i_a = I_p \sin(\omega_e t + \phi_0) = I_p \sin(\phi) \\ i_b = I_p \sin(\omega_e t + \phi_0 - \frac{2}{3}\pi) = I_p \sin(\phi - \frac{2}{3}\pi) \\ i_c = I_p \sin(\omega_e t + \phi_0 + \frac{2}{3}\pi) = I_p \sin(\phi + \frac{2}{3}\pi) \end{cases} \tag{6}$$

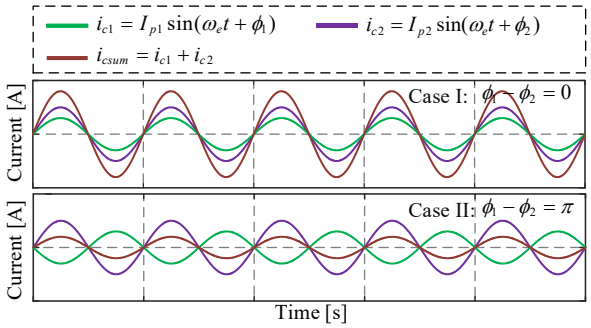

Fig. 4. Confluence of phase current in common leg.

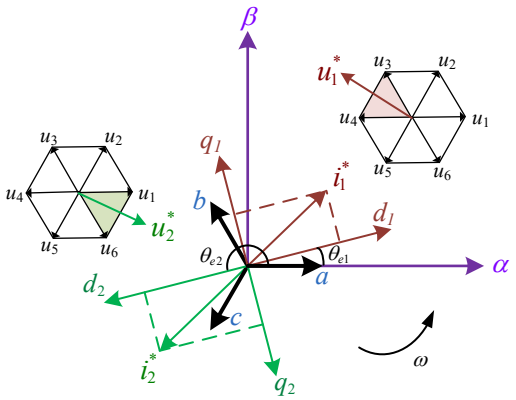

Fig. 5. Position of current vectors and reference VVs.

where I_p is amplitude of current, and ϕ_0 and ϕ are initial phase and time phase respectively.

The currents in α/β coordinate with constant amplitude can be obtained by Clark transform as

$$\begin{bmatrix} i_\alpha \\ i_\beta \end{bmatrix} = \frac{2}{3}\begin{bmatrix} 1 & -1/2 & -1/2 \\ 0 & \sqrt{3}/2 & -\sqrt{3}/2 \end{bmatrix}\begin{bmatrix} i_a & i_b & i_c \end{bmatrix}^T \tag{7}$$

Thus, the expressions of i_α and i_β can be calculated as

$$\begin{cases} i_\alpha = I_p \sin(\phi) \\ i_\beta = -I_p \cos(\phi) \end{cases} \tag{8}$$

Transform the current into d/q coordinate, one can get

$$\begin{cases} i_d = i_\alpha \cos(\theta_e) + i_\beta \sin(\theta_e) = I_p \sin(\phi + \theta_e) \\ i_q = i_\beta \cos(\theta_e) - i_\alpha \sin(\theta_e) = -I_p \cos(\phi - \theta_e) \end{cases} \tag{9}$$

where θ_e is electrical angular position. Therefore, it is apparent that the values of d/q- axis currents depend on the time phase of current and the space angular position of rotor.

The confluence of phase current in common leg enlarges the current and may generate overcurrent. For instance, if the time phases of current are identical of dual PMSMs, the amplitude of current flowing in common leg will be the sum of I_{p1} and I_{p2}, as the case I in Fig. 4. The overcurrent leads to excessive heat, energy loss, and the risk of damage to devices. To suppress the overcurrent in common leg, the current phase difference should be maintained π to match the peak and trough of two current curves, as the case II shown in Fig. 4. When dual PMSMs operate at the same conditions, the current in common leg can be minimized to zero to minimize losses. The traditional methods adopt a position controller to adjust θ_e so as to change ϕ. The position difference is adjusted by PI controller to modify the value of speed reference. As a result,

a triple-loop feedback control structure is established. Under ideal circumstances, the position of current vectors and selected VVs are demonstrated in Fig. 5. When the difference between θ_{e1} and θ_{e2} is maintained as π, the desired VVs of dual PMSMs are located in opposite sectors, which yields the conflict on switching state of leg L_5. To this end, this study adopts a master-slave structure and duty cycle partitioning scheme to realize independent current controller construction. Moreover, the traditional position controller responds slowly due to the cascaded three-loop control structure. Therefore, an improved MPC strategy using current phase difference to directly modify the current reference is also investigated.

B. Cost Function Design

In this scheme, a master-slave structure is adopted to establish the relationship of current phases of dual PMSMs. Two model-based current controllers are employed to select optimal VVs of each PMSM respectively. For master motor, a classical cost function considering the deviation of *d*/*q*-axis currents is used as

$$g_1 = (i_{d1}^* - i_{d1}(k+2))^2 + (i_{q1}^* - i_{q1}(k+2))^2 \tag{10}$$

where (*k*+2) step has considered the one-step delay, and i_{d1}^* and i_{q1}^* are reference values offered from speed controller.

Next, the predictive current generated from the selected VV is transformed to *α*/*β*- axis as

$$\begin{cases} i_{\alpha1}(k+2) = i_{d1}(k+2)*\cos\theta_{e1} - i_{q1}(k+2)*\sin\theta_{e1} \\ i_{\beta1}(k+2) = i_{d1}(k+2)*\sin\theta_{e1} + i_{q1}(k+2)*\cos\theta_{e1} \end{cases} \tag{11}$$

where θ_{e1} is the electric angular position of master motor.

The sine and cosine values of the current phase can be calculated as

$$\begin{cases} \sin(\phi_1) = \dfrac{i_{\alpha1}(k+2)}{I_{p1}(k+2)} \\ \cos(\phi_1) = -\dfrac{i_{\beta1}(k+2)}{I_{p1}(k+2)} \end{cases} \tag{12}$$

where

$$I_{p1}(k+2) = ((i_{\alpha1}(k+2)*i_{\alpha1}(k+2) + (i_{\beta1}(k+2)*i_{\beta1}(k+2))^{1/2} \tag{13}$$

Setting the current phase difference to π, the sine and cosine values of current phase of the slave motor are expected to

$$\begin{cases} \sin(\phi_2) = \sin(\phi_1+\pi) = -\dfrac{i_{\alpha1}(k+2)}{I_{p1}(k+2)} \\ \cos(\phi_2) = \cos(\phi_1+\pi) = \dfrac{i_{\beta1}(k+2)}{I_{p1}(k+2)} \end{cases} \tag{14}$$

Define the reference current obtained from speed controller to slave motor as i_{d2}^* and i_{q2}^*. Since i_d=0 control scheme is utilized, the expected amplitude of the phase current of slave motor can be regarded as i_{q2}^*. Later, based on (14) and to eliminate overcurrent in common leg, the reference current of the slave motor is redistributed in *α*-*β* axis as

$$\begin{cases} i_{\alpha2}^* = i_{q2}^**\sin(\phi_2) = -i_{q2}^*\dfrac{i_{\alpha1}(k+2)}{I_{p1}(k+2)} \\ i_{\beta2}^* = -i_{q2}^**\cos(\phi_2) = -i_{q2}^*\dfrac{i_{\beta1}(k+2)}{I_{p1}(k+2)} \end{cases} \tag{15}$$

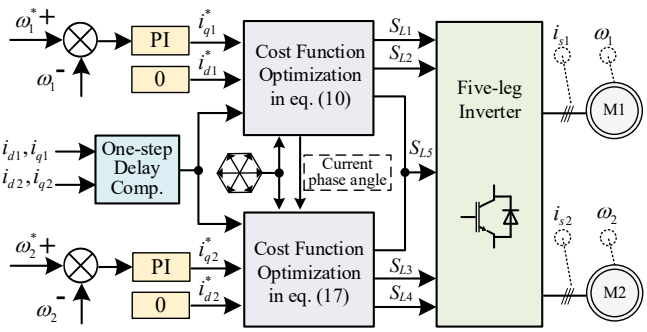

Fig. 6. Block diagram of proposed MPC scheme.

Consequently, the reference current in *d*/*q*- axis is modified to

$$\begin{cases} i_{d2}^{**} = i_{\alpha2}^*\cos(\theta_{e2}) + i_{\beta2}^*\sin(\theta_{e2}) \\ i_{q2}^{**} = i_{\beta2}^*\cos(\theta_{e2}) - i_{\alpha2}^*\sin(\theta_{e2}) \end{cases} \tag{16}$$

where θ_{e2} is the electric angular position of slave motor.

Finally, the basic VVs are substituted into the traversing operation to filter out the optimal vector of the slave motor. The specific cost function is given as

$$g_2 = (i_{d2}^{**} - i_{d2}(k+2))^2 + (i_{q2}^{**} - i_{q2}(k+2))^2 \tag{17}$$

C. Control System Construction

The specific MPC for dual-PMSM drives is derived from the classical approach, but it attaches the consideration of FL-VSI hardware limitation and overcurrent suppression. The whole algorithm is shown in Fig. 6. The PI controller is used as speed controller to generate an initial reference current for dual PMSMs. S_{L1}~S_{L5} are switching commands composited by the outputs of cost function optimization modules. The improved predictive control is designed for current control, the procedure is detailed as follows.

In the first step, a duty ratio scheme based on deadbeat theory is adopted to decouple the relationship of dual-PMSM control, as well as adjust the amplitude of selected basic VVs. The *d*/*q*- axis components and amplitude of expected VV can be calculated as [27]

$$\begin{bmatrix} u_d^* \\ u_q^* \end{bmatrix} = \begin{bmatrix} R_sT_s - L_d & -\omega_e(k)L_qT_s \\ \omega_e(k)L_dT_s & R_sT_s - L_q \end{bmatrix}\begin{bmatrix} i_d(k+1) \\ i_q(k+1) \end{bmatrix} + \begin{bmatrix} L_d & 0 \\ 0 & L_q \end{bmatrix}\begin{bmatrix} i_d^* \\ i_q^* \end{bmatrix} + \begin{bmatrix} 0 \\ \omega_e(k)\psi_f T_s \end{bmatrix}. \tag{18}$$

$$|u^*| = \sqrt{(u_d^*)^2 + (u_q^*)^2}. \tag{19}$$

Thus, the duty ratio of each motor can be given as

$$\begin{cases} \delta_j = \dfrac{|u_j^*|}{2U_{\rm dc}/3}, \delta_0 = 1 - \sum_{j=1}^{2}\delta_j, \text{where} \sum_{j=1}^{2}|u_j^*| > \dfrac{2U_{\rm dc}}{3} \\ \delta_j = \dfrac{|u_j^*|}{\sum_{j=1}^{2}|u_j^*|}, \quad \text{where} \sum_{j=1}^{2}|u_j^*| > \dfrac{2U_{\rm dc}}{3} \end{cases} \tag{20}$$

where $U_{\rm dc}$ is dc-bus voltage.

Secondly, the optimal vector of master PMSM is chosen by using the cost function as (10). Moreover, the u_1^* offers a datum to narrow the range of candidate VVs, only two active

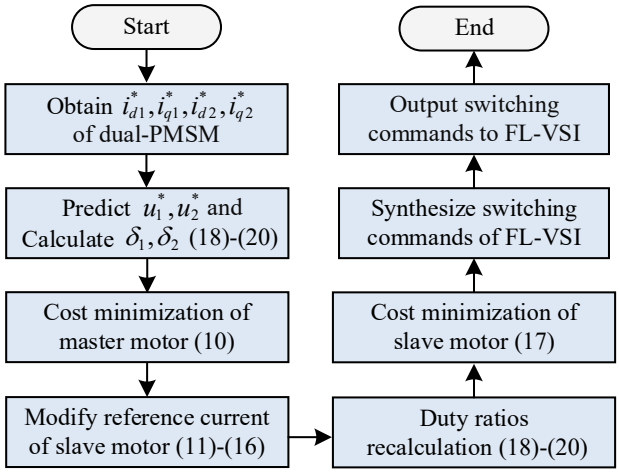

Fig. 7. Flowchart of the improved MPC strategy.

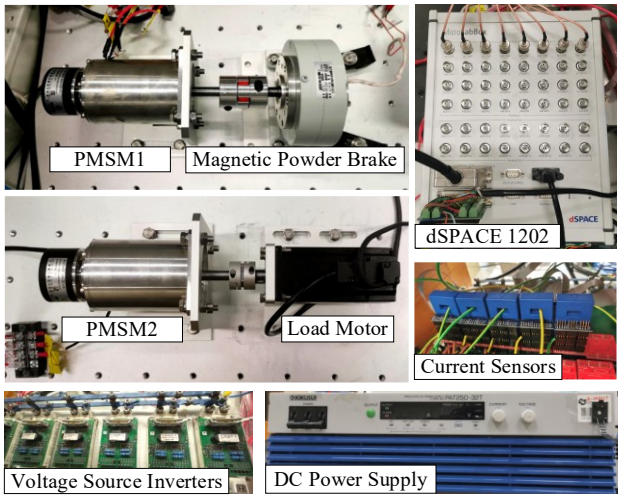

Fig. 8. Test bench.

VVs located as sector boundaries and zero VVs should be explored in (10) with duty ratios from (20). Also, one of the zero vectors (u_0 or u_7) which gives fewer switching commutations is tested.

Thirdly, based on the predictive current of master PMSM under selected VVs and undergoing (11)-(16), the modified reference current of slave PMSM is achieved. This step considers the overcurrent elimination operation.

Fourthly, owing to the change of d/q- axis reference, a repetitive step to calculate the expected voltage of slave motor and redistribute the duty ratios of dual motors via (18)-(20) should be conducted.

Next, similar to the second step, three candidate basic VVs are tested via (2), (3), and (17), and the one that minimizes cost function is selected. Therefore, a total of six candidate VVs are traversed in a control period, which results in a lower computational burden.

Finally, based on the chosen VVs from two cost functions, the switching signals of FL-VSI are composited. The whole flowchart of the proposed MPC scheme is shown in Fig. 7.

IV. Experimental Verification

In this section, the experimental verifications are carried out. The performance of steady-state, dynamic, and algorithm complexity are tested and compared with that under the traditional MPC scheme with settled half-period partition for each motor (denoted as MPC1) and the priority-based MPC strategy (denoted as MPC2) [23]. Moreover, the effectiveness of overcurrent suppression is further compared with the angle controller-based method [27].

A. Experimental Setup

The test bench is shown in Fig. 8, which consists of a dSPACE DS1202 controller, IGBTs, current sensors, and the required power supply. The parameters of dual PMSMs are identical and listed in Table I. The deviations of actual values and nominal values are regarded as disturbances. A magnetic powder clutch and a servo motor are employed as different loads. The phases c of dual motors are connected and the five IGBT-based legs are used in the test. Besides, the control frequency and dc-bus voltage are given as 20 kHz and 64V, respectively. The parameters of speed PI controllers are empirically tuned to achieve optimal control performance. In the proposed scheme, the M1 is selected as the master motor. In the compared angle controller, the proportional and integral coefficients of PI controller are 50 and 6 respectively.

TABLE I
Main Parameters of PMSMs

Items	Quantity	Value
n_N (r/min)	Rated speed	1000
T_N (N·m)	Rated torque	2
L_d (mH)	Direct Inductance	3.7
L_q (mH)	Quadrature Inductance	5
ψ_f (Wb)	Magnet flux linkage	0.055
R_s (Ω)	Stator resistance	0.9
J (kg·m^2)	Rotational inertia	5x10^{-5}
p	Pole pairs	5

B. Steady-State Performance

The steady-state performance under three methods is shown in Fig. 9. Owing to the division of control period, the voltage applied to each PMSM reduces inevitably. Consequently, all experimental tests are conducted at lower conditions than rated ones. In Fig. 9, the dual PMSMs operate steadily at the identical conditions of 400 r/min with 1 N·m load. It can be observed that the MPC2 scheme yields the highest speed fluctuation, current ripple, and torque ripple. The total harmonic distortions (THDs) of phase current of dual PSMSMs rise to 12.75% and 12.17%, respectively. This scheme offers higher voltage utilization because it can output active VVs to dual PMSMs simultaneously. However, it cannot adjust the amplitudes of applied VVs, which decreases control accuracy inevitability. Similar to MPC2, the MPC1 scheme with half-period partition also generates the VVs with constant magnitudes. Nevertheless, in each partition, eight basic VVs are explored in related cost functions to select the optimal solution, which decouples dual PMSMs completely. As a result, the THD values reduce to 7.77 % and 7.47%, and the torque ripple decreases to 0.37 N·m.

In addition, the proposed MPC strategy possesses similar steady-state performance compared with the MPC1 scheme, in which the THDs are 7.39% and 7.63%, and the torque ripple is 0.41 N·m. However, it can eliminate the overcurrent of the

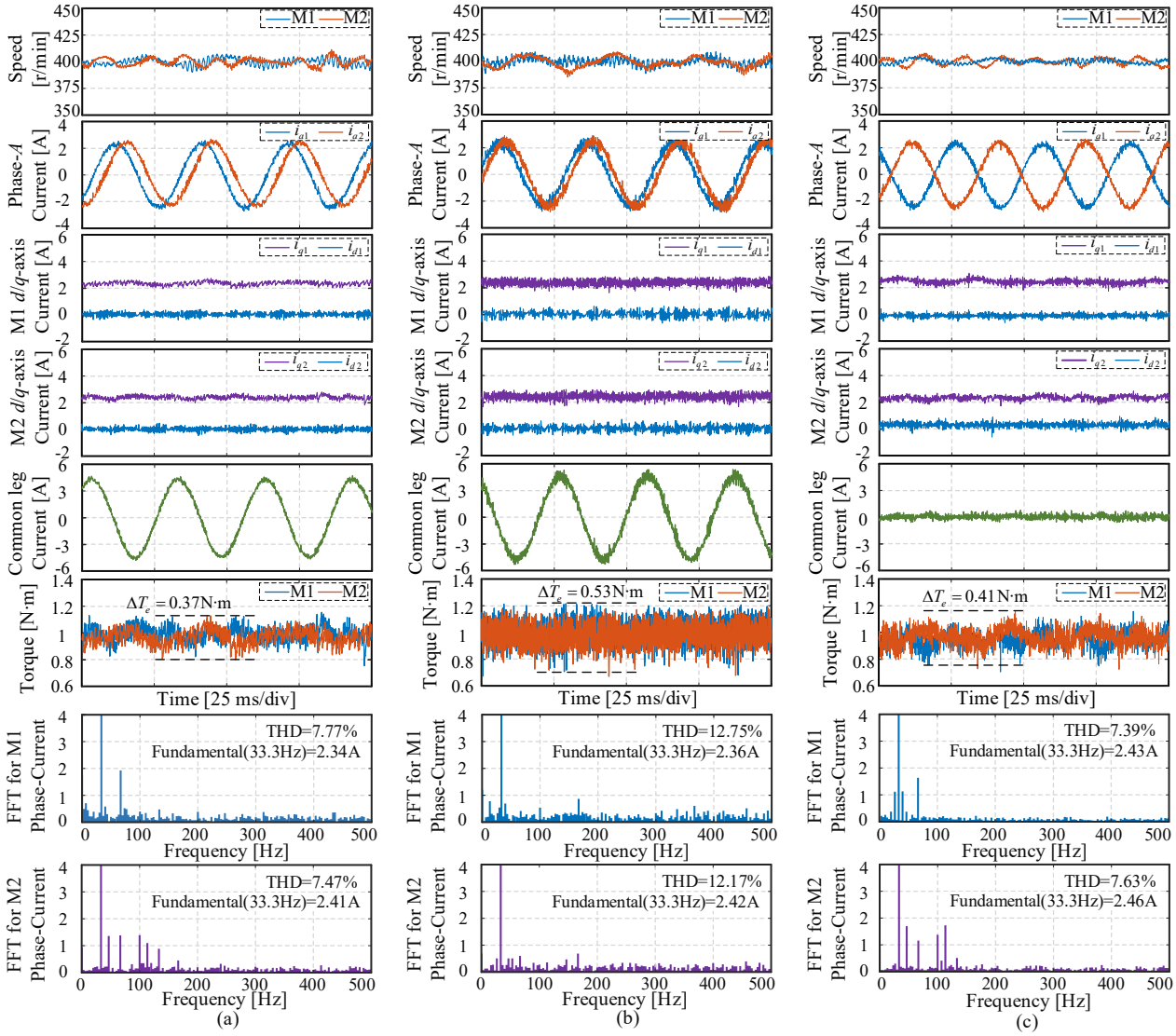

Fig. 9. Steady-state performance comparison. The reference speed and applied load torque of dual PMSMs are 400 r/min and 1 N·m. (a) Traditional MPC1 scheme. (b) Improved MPC2 scheme. (c) Proposed MPC scheme.

sharing leg at the same time. The difference of the current phase maintains as π. The current in L_5 is minimized to zero, in contrast to alternative schemes where currents reach up to 5 A. The switching losses under the three methods are 6.87 W, 6.64 W, and 6.15 W, respectively. Therefore, the proposed scheme results in less energy loss and reduces the capacity requirements for switches. Moreover, it can be observed that though the i_d reference of slave motor is calculated via (16), it remains at zero steadily. Thanks to the accurate position and current measurement, and the high sample frequency, the i_d can track reference value quickly without heavy fluctuation.

C. Dynamic Performance

A dynamic test under step load is conducted and the results are demonstrated in Fig. 10. The three schemes all offer fast dynamic response, namely the speed of M2 drops from 400 r/min to nearly 350 r/min and recovers to the initial speed within 10 ms, which inherits the inherent superiority of predictive control. The i_{q2} increases rapidly when the step load appears and i_{d2} stays at 0. In the proposed MPC scheme, the difference of electrical angular position keeps at π, thus, the current in common leg can stay at the minimum. On the contrary, the differences are uncontrolled at MPC1 and MPC2 strategies, and the overcurrent in common leg increases to 5A.

Another group of experimental results under the step speed test of dual PMSMs is presented in Fig. 11. The detailed comparisons of speed overshoot, rise time, settling time, and the peak value of common leg current are listed in Table II. The rise time is defined as the time required for speed signal to increase from 0% to 100% of the waveform. The settling time refers to the time for speed error to converge to 2.5% of the final value. It can be observed that there is a negative correlation between speed overshoot and rise time. In the proposed scheme, the dynamic duty cycle partitioning ensures a fast transient response of master motor. Compared to MPC1 and MPC2 schemes, the rise time of M1 reduces from 10.92 ms and 10.65 ms to 10.35 ms. In addition, the slave motor presents less overshoot and slight larger rise time. However, it shows the smallest settling time compared to its counterparts.

Furthermore, it should be mentioned that there is a bulge in i_{d2} curve when the speed steps up under the proposed scheme, which is generated from the fluctuation of master motor

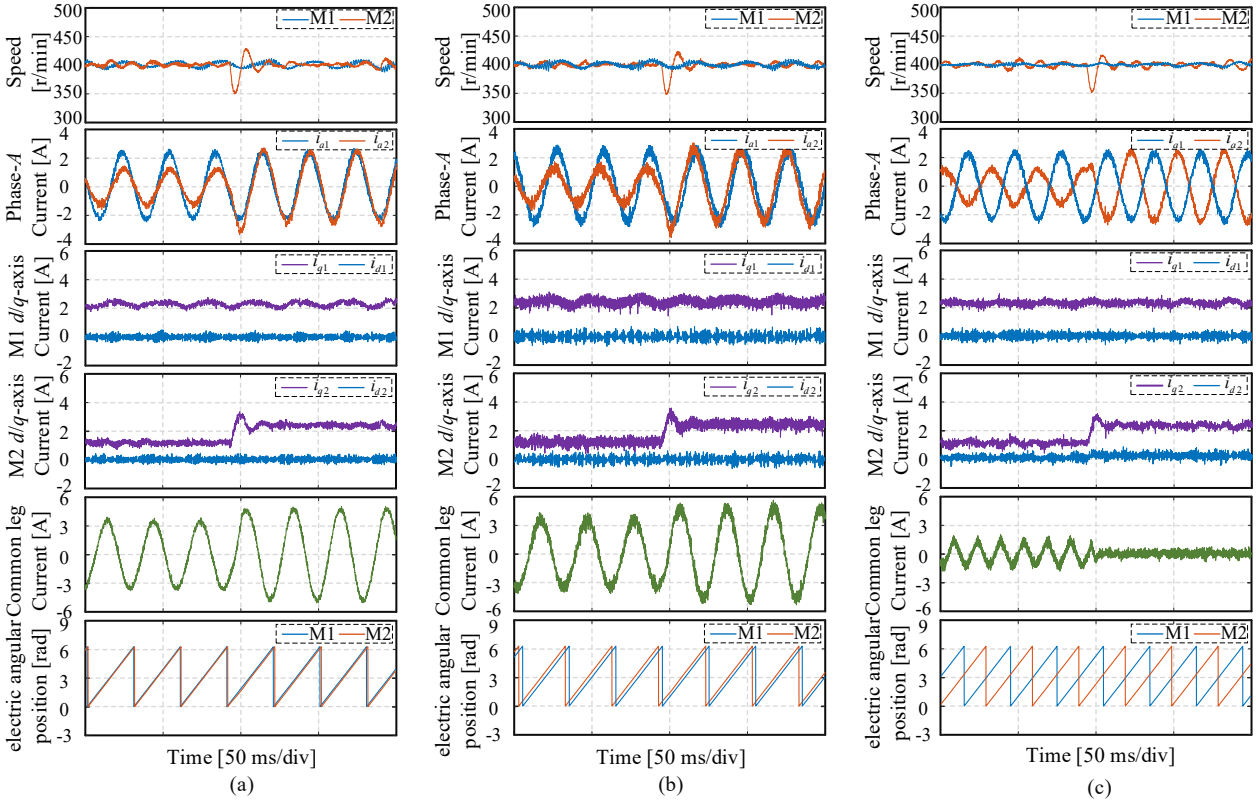

Fig. 10. Dynamic performance at step load. M1 runs at 400 r/min with 1 N·m load, while a step load torque from 0.5 N·m to 1 N·m is applied to M2. (a) Traditional MPC1 scheme. (b) Improved MPC2 scheme. (c) Proposed MPC scheme.

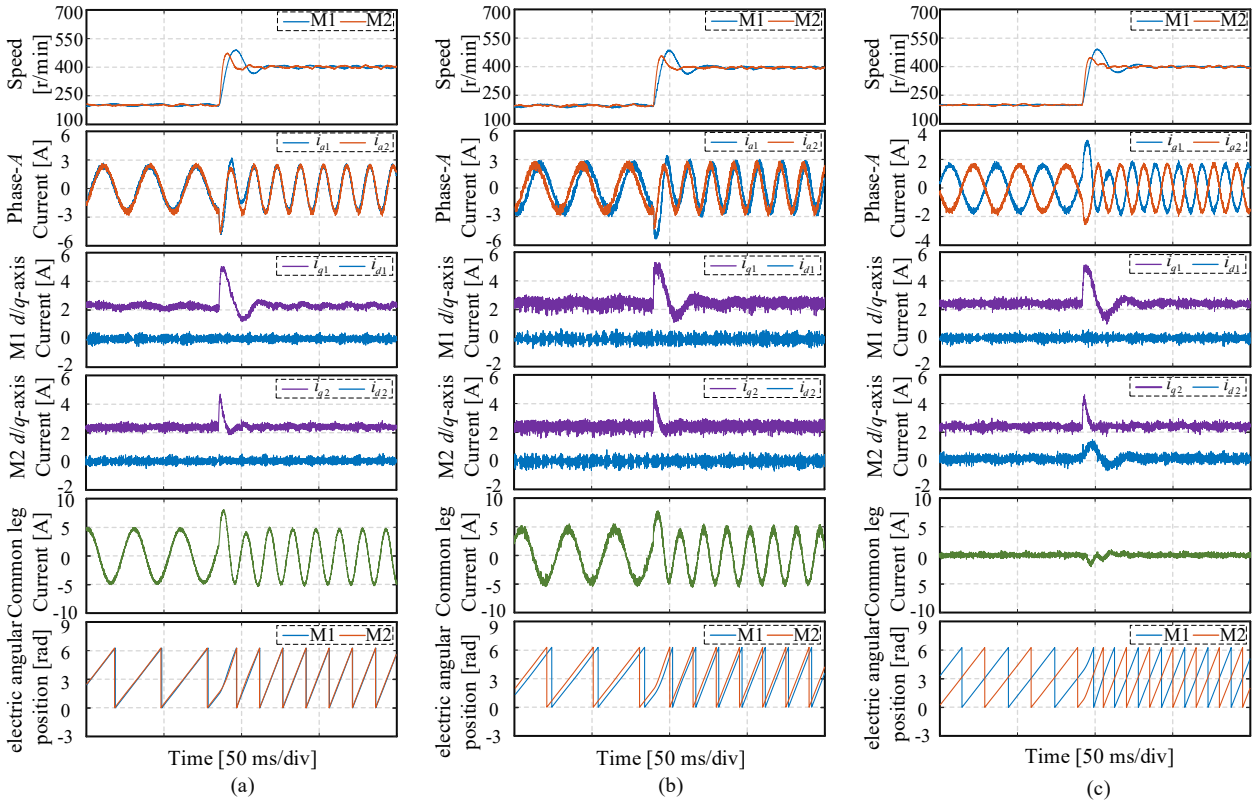

Fig. 11. Dynamic performance at step speed. A step speed reference from 200 r/min to 400 r/min. Load torque is 1 N·m. (a) Traditional MPC1 scheme. (b) Improved MPC2 scheme. (c) Proposed MPC scheme.

current. Nevertheless, i_{d2} can converge to zero fast due to the effective adjustment of the currents of dual PMSMs and will not worsen algorithm performance. Moreover, the higher sampling and control frequencies and sufficient voltage supply can help remove the fluctuation of i_{d2}. In addition, the proposed MPC scheme suppresses the overcurrent in common

TABLE II
COMPARISON OF STEP SPEED EXPERIMENT

Items	MPC1		MPC2		Proposed MPC	
	M1	M2	M1	M2	M1	M2
Speed overshoot (r/min)	89.79	72.89	93.12	61.72	93.52	49.19
Percent overshoot (%)	19.95	18.22	23.28	15.43	23.38	12.30
Rise time (ms)	10.92	5.23	10.65	5.15	10.35	5.42
Settling time (ms)	55.11	32.58	56.13	35.15	54.81	29.11
Absolute peak of i_{L5} (A)	8.10		7.88		1.08	

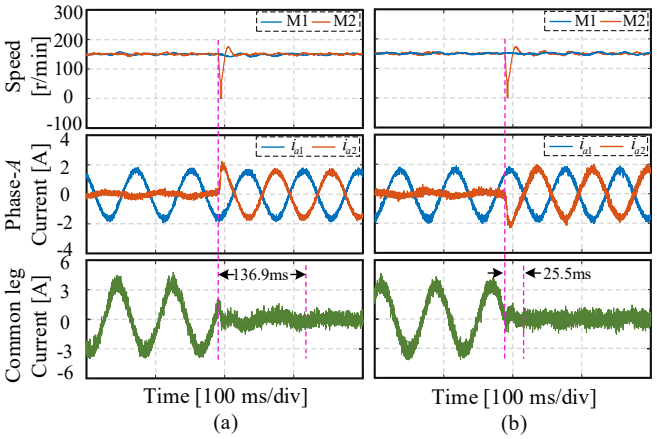

Fig. 12. Comparison of overcurrent elimination under step load. Dual PMSMs run at 150 r/min. The load of M1 is 1 N·m and a step load from 0 to 1 N·m is applied to M2. (a) MPC1 with angle controller. (b) Proposed MPC scheme.

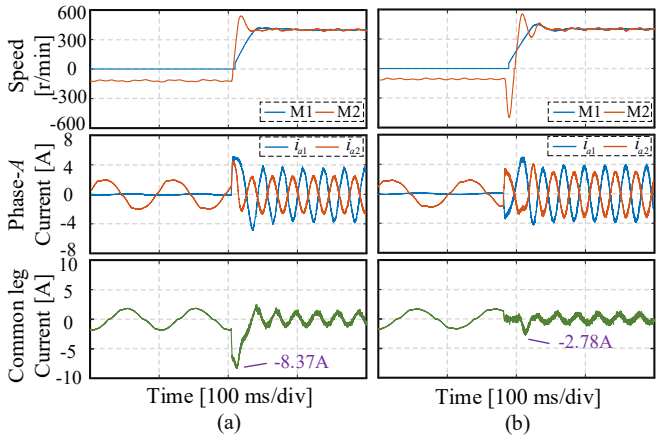

Fig. 13. Comparison of overcurrent elimination under start-up. The speed reference is 400 r/min. Loads of dual PMSMs are 1.5 N·m and 1 N·m. (a) MPC1 with angle controller. (b) Proposed MPC scheme.

TABLE III
COMPARISON OF STRUCTURES AND PERFORMANCE

Index of comparison	MPC1	MPC2 [23]	Proposed MPC
Traversed VVs in a control period	16	12	6
Computational time (μs)	41.6	37.2	35.1
Voltage utilization	Low	High	Low
Amplitude of common leg current	Large	Large	Small

leg effectively when motors speed up. The absolute peak value of i_{L5} is minimized to 1.08 A. Compared to MPC1 and MPC2 methods, it is reduced by 86.67% and 86.29%. To sum up, the proposed scheme realizes effective overcurrent elimination and fast transient response simultaneously.

D. Overcurrent Elimination Comparison

The comparisons of overcurrent elimination of the proposed MPC scheme and the MPC1 method with angle controller [27] are presented in this section. Firstly, the comparison under step load is conducted. The experimental results of speed, phase current, and common leg current are shown in Fig. 12. It can be seen that both strategies realize overcurrent suppression of common leg. The PI controller-based angle controller can adjust the electrical angular position to suppress the overcurrent flowing in common leg. Nevertheless, it responds more slowly than the proposed predictive scheme. In comparison, the proposed scheme diminishes the time required for the stable convergence of current from 136.9 ms to 25.5 ms, representing a reduction of 81.37%.

Moreover, the experimental results of on-load start-up test are demonstrated in Fig. 13. The dual PMSMs give different speed rise curves due to the various load characteristics. The conventional strategy presents fast dynamic response, but the transient overcurrent appears in common leg. On the contrary, the proposed approach can eliminate the transient overcurrent by adjusting the motor speed of dual PMSMs quickly and adaptively, including the reversal of motor. Compared to the traditional scheme, the amplitude of overcurrent is reduced from 8.37 A to 2.78 A, which is dramatically reduced by 66.79%. Therefore, the step-load and start-up experiments verify the superiority of the proposed overcurrent elimination method.

E. Complete Performance Discussion

In addition to steady-state and dynamic performance, some other indexes, such as computational time and voltage utilization, are compared in this section. The comparison results are listed in Table III. Firstly, since the MPC1 method traverses 16 VVs, it consumes the longest computational time as 41.6 μs. However, the proposed scheme reduces the number of candidate VVs to 6, thus it decreases the time to 35.1μs. Among the three methods, the MPC2 possesses the highest voltage utilization at the cost of higher current ripple. Conversely, MPC1 and the proposed MPC

strategies realize decoupled control of dual PMSMs via using the duty cycle partitioning method, but they reduce voltage utilization inevitably. Furthermore, the proposed method suppresses the overcurrent in common leg particularly.

Moreover, it should be mentioned that there are some identical characteristics of the three methods, such as simple parameter design and high model dependence. The parameter mismatches may deteriorate the control performance heavily. To this end, the other advanced control algorithms, such as parameter identification and observer-based technologies, can be combined with the proposed MPC scheme for enhanced performance.

V. Conclusion

This paper proposes a novel predictive control scheme to realize the excellent cooperative control of a dual-PMSM system supplied by FL-VSI. The deadbeat control-based duty cycle partitioning scheme is adopted to realize independent current controller construction. The master-slave structure is incorporated into the MPC frame considering the relations of current phases of dual PMSMs. The overcurrent is eliminated by a new cost function, where the current reference of slave motor is modified. A case study was conducted on a dual-PMSM system to experimentally test and compare the proposed control scheme with the classical ones. The results prove that the proposed approach inherits fast transient response, reduces current ripple, and enables effective overcurrent suppression.

To sum up, this approach has promising potential for cooperative control by FL-VSI topology in dual-PMSM parallel applications, such as electric tractions, conveyor belts, and paper machines. In future work, the general strategies for multi-motor parallel drives with stronger robustness can be further investigated.

References

[1] S. Ok, J. Bae, and D.-H. Lee, "Curving motion control of a traction rail mover using a dual blac motor drive," *IEEE Transactions on Industry Applications,* vol. 59, no. 1, pp. 1175-1183, 2023, doi: 10.1109/tia.2022.3204240.

[2] Y. Song, J. Zhao, J. Sun, and Y. Zhou, "Model predictive vector control for four-switch mono-inverter dual im system," *IEEE Transactions on Power Electronics,* vol. 38, no. 1, pp. 396-405, 2023, doi: 10.1109/tpel.2022.3206957.

[3] Y. Chen, C. Liu, W. Wang, and S. Liu, "Predictive flux weakening control of pmsms supplied from reduced-switch-count vsi," *IEEE/ASME Transactions on Mechatronics,* pp. 1-11, 2024, doi: 10.1109/tmech.2024.3360189.

[4] C. Yang, F. Meng, H. Zhang, J. Zhao, H. Wang, and L. Zhou, "Optimal coordinated control for speed tracking and torque synchronization of rigidly connected dual-motor systems," *IEEE/ASME Transactions on Mechatronics,* vol. 28, no. 5, pp. 2609-2620, 2023, doi: 10.1109/tmech.2023.3242663.

[5] B. Jung, P. Jang, K. Nam, and Y. Kim, "Overmodulation strategy for torque balance of dual-motor systems considering angle offset," *IEEE Transactions on Industry Applications,* vol. 58, no. 6, pp. 6869-6878, 2022, doi: 10.1109/tia.2022.3198382.

[6] R. Huang, Z. Dong, Z. Song, and C. Liu, "A novel counter-rotating afpm machine based on magnetic-field modulation for underwater propulsion system," *IEEE Transactions on Industrial Electronics,* vol. 71, no. 3, pp. 2167-2176, 2024, doi: 10.1109/tie.2023.3270515.

[7] Y. Chen, C. Liu, S. Liu, and Y. Liu, "Predictive control scheme with adaptive overmodulation for a five-leg vsi driving dual pmsms," *IEEE Transactions on Industrial Electronics,* vol. 71, no. 1, pp. 71-81, 2024, doi: 10.1109/tie.2023.3245221.

[8] W. Wang, Y. Liu, Y. Chen, and C. Liu, "Optimization-based duty cycle allocation for a five-leg inverter to drive two electric motors," *IEEE Transactions on Power Electronics,* vol. 38, no. 9, pp. 11327-11337, 2023, doi: 10.1109/tpel.2023.3287469.

[9] W. Wang, M. Cheng, B. Zhang, Y. Zhu, and S. Ding, "A fault-tolerant permanent-magnet traction module for subway applications," *IEEE Transactions on Power Electronics,* vol. 29, no. 4, pp. 1646-1658, 2014, doi: 10.1109/tpel.2013.2266377.

[10] S. Ito, T. Moroi, Y. Kubo, K. Matsuse, and K. Rajashekara, "Independent control of two permanent-magnet synchronous motors fed by a four-leg inverter," *IEEE Transactions on Industry Applications,* vol. 51, no. 1, pp. 753-760, 2015, doi: 10.1109/tia.2014.2332637.

[11] J. Lee and J.-W. Choi, "Mtpa control method for midp spmsm drive system using angle difference controller and p&o algorithm," *IEEE Transactions on Power Electronics,* vol. 37, no. 12, pp. 15382-15396, 2022, doi: 10.1109/tpel.2022.3196400.

[12] W. Wang, J. Zhang, and M. Cheng, "A dual-level hysteresis current control for one five-leg vsi to control two pmsms," *IEEE Transactions on Power Electronics,* vol. 32, no. 1, pp. 804-814, 2017, doi: 10.1109/tpel.2016.2535294.

[13] Q. Geng *et al.*, "An improved pwm method of five-leg vsi fed dual-pmsm system with duty cycles regulation," *IEEE/ASME Transactions on Mechatronics,* vol. 27, no. 6, pp. 5771-5779, 2022, doi: 10.1109/tmech.2022.3190690.

[14] C. S. Lim, N. A. Rahim, W. P. Hew, and E. Levi, "Model predictive control of a two-motor drive with five-leg-inverter supply," *IEEE Transactions on Industrial Electronics,* vol. 60, no. 1, pp. 54-65, 2013, doi: 10.1109/tie.2012.2186770.

[15] Q. Geng, Z. Li, M. Zhang, Z. Zhou, H. Wang, and T. Shi, "Sensorless control method for dual permanent magnet synchronous motors driven by five-leg voltage source inverter," *IEEE Journal of Emerging and Selected Topics in Power Electronics,* vol. 10, no. 1, pp. 260-272, 2022, doi: 10.1109/jestpe.2021.3096198.

[16] Q. Geng, J. He, Z. Yu, G. Zhang, and Z. Zhou, "Current reconstruction for dual pmsms fed by a five-leg voltage source inverter with a single current sensor," *IEEE Transactions on Energy Conversion,* vol. 38, no. 1, pp. 479-494, 2023, doi: 10.1109/tec.2022.3208158.

[17] D. Dujic, M. Jones, S. N. Vukosavic, and E. Levi, "A general pwm method for a (2n + 1) -leg inverter supplying n three-phase machines," *IEEE Transactions on Industrial Electronics,* vol. 56, no. 10, pp. 4107-4118, 2009, doi: 10.1109/tie.2009.2014909.

[18] J. Riccio, P. Karamanakos, S. Odhano, M. Tang, M. D. Nardo, and P. Zanchetta, "Direct model predictive control of synchronous reluctance motor drives," *IEEE Transactions on Industry Applications,* vol. 59, no. 1, pp. 1054-1063, 2023, doi: 10.1109/tia.2022.3213002.

[19] R. Huang, Z. Dong, B. Zhang, and C. Liu, "Decoupled modulation strategy for harmonic current suppression in five-phase series-end winding pmsm drives," *IEEE Transactions on Industrial Electronics,* pp. 1-6, 2024, doi: 10.1109/tie.2024.3349582.

[20] W. Xu, Y. Tang, D. Dong, X. Xiao, E. E. M. Rashad, and A. K. Junejo, "Optimal reference primary flux based model predictive control of linear induction machine with mtpa and field-weakening operations for urban transit," *IEEE Transactions on Industry Applications,* vol. 58, no. 4, pp. 4708-4721, 2022, doi: 10.1109/tia.2022.3166458.

[21] C.-S. Lim, E. Levi, M. Jones, N. A. Rahim, and W.-P. Hew, "A comparative study of synchronous current control schemes based on fcs-mpc and pi-pwm for a two-motor three-phase drive," *IEEE Transactions on Industrial Electronics,* vol. 61, no. 8, pp. 3867-3878, 2014, doi: 10.1109/tie.2013.2286573.

[22] C.-S. Lim, E. Levi, M. Jones, N. A. Rahim, and W.-P. Hew, "A fault-tolerant two-motor drive with fcs-mp-based flux and torque control," *IEEE Transactions on Industrial Electronics,* vol. 61, no. 12, pp. 6603-6614, 2014, doi: 10.1109/tie.2014.2317135.

[23] D. Choi, J.-S. Lee, Y.-S. Lim, and K.-B. Lee, "Priority-based model predictive control method for driving dual induction motors fed by five-leg inverter," *IEEE Transactions on Power Electronics,* vol. 38, no. 1, pp. 887-900, 2023, doi: 10.1109/tpel.2022.3203961.

[24] J. Liu, J. Yang, S. Li, and X. Wang, "Single-loop robust model predictive speed regulation of pmsm based on exogenous signal preview," *IEEE Transactions on Industrial Electronics,* vol. 70, no. 12, pp. 12719-12729, 2023, doi: 10.1109/tie.2023.3239938.

[25] A. Brosch, O. Wallscheid, and J. Böcker, "Time-optimal model predictive control of permanent magnet synchronous motors considering current and torque constraints," *IEEE Transactions on Power*

Electronics, vol. 38, no. 7, pp. 7945-7957, 2023, doi: 10.1109/tpel.2023.3265705.

[26] Y. Wang, H. Yu, and Y. Liu, "Speed-current single-loop control with overcurrent protection for pmsm based on time-varying nonlinear disturbance observer," *IEEE Transactions on Industrial Electronics,* vol. 69, no. 1, pp. 179-189, 2022, doi: 10.1109/tie.2021.3051594.

[27] Y. Chen, C. Liu, H. Wen, and Z. Dong, "Improved model predictive control for multimotor system using reduced-switch-count vsi with current minimization," *IEEE Transactions on Power Electronics,* vol. 38, no. 7, pp. 8786-8797, 2023, doi: 10.1109/tpel.2023.3267116.

[28] Y. Chen, Z. Dong, Z. Song, and C. Liu, "Predictive control of five-leg inverter driving dual pmsms for overcurrent suppression," in *2023 IEEE 6th Student Conference on Electric Machines and Systems (SCEMS)*, 7-9 Dec. 2023, pp. 1-5, doi: 10.1109/SCEMS60579.2023.10379328.

[29] T. Li, X. Sun, G. Lei, Y. Guo, Z. Yang, and J. Zhu, "Finite-control-set model predictive control of permanent magnet synchronous motor drive systems—an overview," *IEEE/CAA Journal of Automatica Sinica,* vol. 9, no. 12, pp. 2087-2105, 2022, doi: 10.1109/jas.2022.105851.

Yong Chen (S'21) received the B.Eng. and M.Eng. degrees in electrical engineering from Southeast University, Nanjing, China, in 2017 and 2020, respectively. He is currently working toward the Ph.D. degree in electrical and electronic engineering at the City University of Hong Kong, Hong Kong, SAR

His main research interests include advanced control of motor drive systems and multi-motor systems.

Zhiping Dong (S'21–M'24) received his Ph.D. degree in electrical and electronic engineering from the City University of Hong Kong, Hong Kong SAR, China, in 2024. Currently, he serves as the Postdoc Fellow in School of Energy and Environment, City University of Hong Kong.

His research interests focus on multi-phase motor drives, hetero-topology converters, and fault-tolerant control.

Chunhua Liu (M'10–SM'14) received the B.Eng. and M.Eng. degrees in Automatic Control from Beijing Institute of Technology, China, and Ph.D. degree in Electrical and Electronic Engineering from The University of Hong Kong, Hong Kong SAR, in 2002, 2005 and 2009, respectively.

Currently, he serves as a Professor in Electrical and Electronic Engineering with the School of Energy and Environment, City University of Hong Kong, Hong Kong SAR, China. His research interests include electric machines and drives, electric vehicles and aircrafts, electric robotics and ships, renewables and microgrids, power electronics and wireless power transfer. In these areas, he has published over 300 refereed papers. In addition, he is an RGC Research Fellow, Distinguish Lecturer of IEEE Vehicular Technology Society (VTS), and World's Top 2% Scientists according to metrics compiled by Stanford University.

Prof. Liu is now an Associate Editor of IEEE Transactions on Industrial Electronics, Editor of IEEE Transactions on Vehicular Technology, Editor of IEEE Transactions on Energy Conversion, and Editor of IEEE Power Engineering Letters. Also, he is an Editor of Energies, Subject Editor of IET – Renewable Power Generation, Associate Editor of Open Journal of the Industrial Electronics Society, Associate Editor of IEEE Access; Associate Editor of IEEE Chinese Journal of Electrical Engineering, Associate Editor of CES Transactions on Electrical Machines and Systems, Associate Editor of Elsevier Green Energy and Intelligent Transportation, and Editor of IEEE Transactions on Magnetics – Conference, respectively. In addition, he is Chair & Founder of both Hong Kong Chapter, IEEE Vehicular Technology Society, and Hong Kong & Guangzhou Joint Chapter, IEEE Industrial Electronics Society, respectively.

Zaixin Song (M'21) received the B.Eng. and M.Eng. degrees in electrical engineering and automation at Harbin Institute of Technology (HIT), Harbin, China, in 2016 and 2018, respectively. He received the Ph.D. degree majoring electrical engineering at City University of Hong Kong (CityU), Hong Kong, in 2021. In September 2021, he worked as a postdoctoral research fellow in CityU. In July 2022, he worked as a postdoctoral research fellow in Nanyang Technological University, Singapore. Currently, he is working as a Research Assistant Professor in State Key Laboratory of Ultra-precision Machining Technology (SKL-UMT), Department of Industrial and Systems Engineering at The Hong Kong Polytechnic University.

Dr. Song has been working on electric machinery for years. His current research interests include Electric Motor Design & Control, Sustainable Energy Conversion & Management, Smart Manufacturing & Robotics Drives, Sustainable Propulsion, among other related fields. His expertise lies in the reliability design of electric machines and multiphysics modeling.